Hybrid microfiber–lithium-niobate nanowaveguide structures as high-purity heralded single-photon sources

Philip Main,[1] Peter J. Mosley,[1] Wei Ding,[2,*] Lijian Zhang,[3,4] and Andrey V. Gorbach[1,†]

[1]*Centre for Photonics and Photonic Materials, Department of Physics, University of Bath, Bath BA27AY, United Kingdom*

[2]*Institute of Physics, Chinese Academy of Sciences, Beijing 100190, China*

[3]*National Laboratory of Solid State Microstructures and College of Engineering and Applied Sciences, Nanjing University, Nanjing 210093, China*

[4]*Collaborative Innovation Center of Advanced Microstructures, Nanjing University, Nanjing 210093, China*

(Received 25 July 2016; published 19 December 2016)

We propose a compact, fiber-integrated architecture for photon-pair generation by parametric downconversion with unprecedented flexibility in the properties of the photons produced. Our approach is based on a thin-film lithium niobate nanowaveguide, evanescently coupled to a tapered silica microfiber. We demonstrate how controllable mode hybridization between the fiber and waveguide yields control over the joint spectrum of the photon pairs. We also investigate how independent engineering of the linear and nonlinear properties of the structure can be achieved through the addition of a tapered, proton-exchanged layer to the waveguide. This allows further refinement of the joint spectrum through custom profiling of the effective nonlinearity, drastically improving the purity of the heralded photons. We give details of a source design capable of generating heralded single photons in the telecom wavelength range with purity of at least 0.95, and we provide a feasible fabrication methodology.

DOI: 10.1103/PhysRevA.94.063844

Quantum technologies promise to deliver functionality not possible with classical paradigms employed in computation, communication, and measurement [1]. Photonic quantum-information processing shows great merit due to the relative simplicity of the components required and the capability to operate in ambient conditions [2,3]. However there are several key challenges to solve before photonic quantum technologies can be scaled up to demonstrate extensive real-world impact, most notably the design of more effective sources of single photons.

Considerable progress has been made in developing sources of heralded single photons based on spontaneous parametric downconversion (SPDC) in which photon pairs are generated as a pump laser propagates through a nonlinear crystal [4]. These sources are attractive not only due to their ability to deliver high count rates but also because they work at room temperature and pressure. Early implementations used free-space components [5,6]; however the drive towards integrated optics has led to the development of guided-wave SPDC sources that demonstrate higher efficiencies and require lower pump powers [7,8].

Despite their success these approaches have their limitations. Integration of SPDC sources into large-scale devices requires miniaturization, and even in fiber-pigtailed waveguide devices the periodic poling required to achieve phase matching imposes a minimum device length of several millimeters. Furthermore, waveguide out-coupling efficiency can be limited as the photon pairs produced often do not match well to single-mode optical fiber [9]. Although the issue of miniaturization can be addressed with sources based on spontaneous four-wave mixing in materials compatible with established microfabrication techniques (for example, silicon-on-insulator), the third-order nonlinearity available is orders of magnitude smaller, limiting count rates and necessitating complex device designs to maximize effective interaction length, inevitably increasing losses [10,11].

Furthermore, the intrinsic energy and momentum conservation associated with SPDC typically results in anticorrelation between the frequencies of the daughter photons. This provides distinguishing information that yields a mixed state when one photon is detected to herald the presence of its twin [12]. Although frequency correlation can be removed by tight filtering, to preserve high count rates the photon pairs can be tailored by controlling the dispersion of the nonlinear medium. This enables frequency correlation to be minimized at the point of generation to produce high-purity heralded photons [13], as demonstrated both in bulk crystals and quasi-phase-matched waveguides [14–18]. However, control over an additional degree of freedom—the magnitude of the nonlinearity—is required to achieve the ultimate purity. For example, modulating the duty cycle of periodically poled waveguides can produce apodization of the effective nonlinearity in the direction of propagation at the cost of significantly reduced effective interaction length and longer devices [19,20].

In this work we show that planar nanostructuring in the transversal, rather than the longitudinal, dimension [21] offers a more elegant approach to design ultracompact and efficient SPDC sources of heralded photons. Our scheme is based on mode hybridization of a lithium niobate thin-film (LNOI) [22] nanowaveguide with an integrated shallow proton-exchanged (PE) channel [23] and a silica microfiber [21], as shown in Fig. 1. This structure enables the unique combination of high nonlinearity of LNOI, the ability to engineer dispersion and nonlinearity independently, and natural integration with low-loss fiber optic systems.

The hybrid structure can be prepared with the help of well-established nanofabrication techniques. After lithographically defining a PE channel of a fixed depth ($d = 0.16\ \mu$m) and variable width $w(y)$ [23] on an X-cut LNOI wafer (of thickness $H = 0.3\ \mu$m) [22,24,25], a "floating" nanoscale waveguide

*wding@iphy.ac.cn

†A.Gorbach@bath.ac.uk

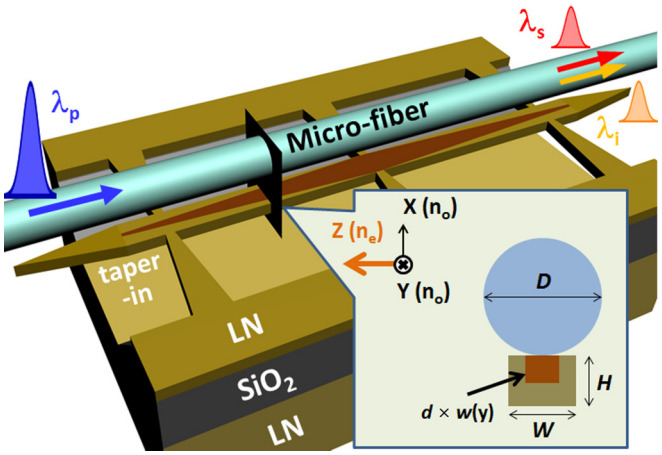

FIG. 1. Microfiber-nanowaveguide hybrid structure: A silica microfiber of diameter D is attached to a "floating" LN waveguide of height H and width W. The additional proton-exchanged channel of height d and variable width $w(y)$ is introduced in the waveguide.

with constant width W can be fabricated by focused ion-beam milling, followed by HF wet etching. A silica microfiber with diameter D is attached on top of the waveguide. Van der Waals attraction is then used to keep together the whole structure and align the fiber and the waveguide symmetrically. When necessary, the fiber can be detached and reassembled at other positions [21].

In our scheme, the SPDC process occurs between a particular set of guided modes of the hybrid structure, i.e., from a short-wavelength pulse in a higher-order mode (pump) to a pair of long-wavelength photons in their fundamental modes (signal and idler) (see Fig. 2). Using the tapering-in

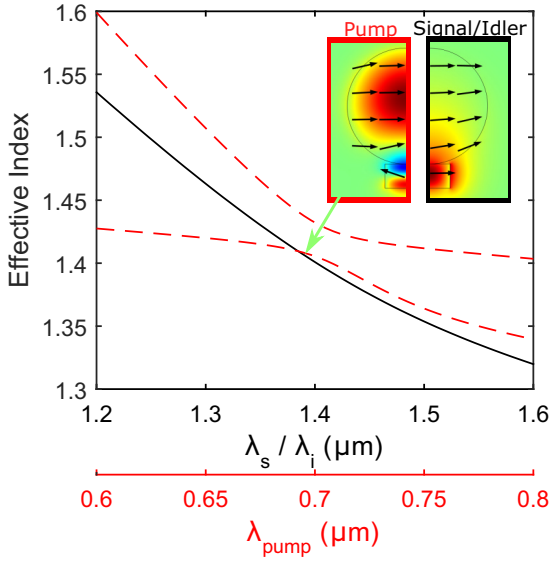

FIG. 2. Effective index ($n_{\text{eff}} = 2\pi\beta/\lambda$) for degenerate signal and idler modes ($\omega_s = \omega_i$, solid black line) and pump modes (red dashed line) for a structure with $D = 1.44$ μm and $W = 0.51$ μm. Phase matching $\Delta\beta = 0$ occurs at intersection points. See inset for polarization (indicated by arrows) and the z component of the electric field of the two modes at the phase-matching point.

and -out geometries of the waveguide (see Fig. 1), the pump and the signal and idler modes can be adiabatically converted to the TE_{01} and the HE_{11} modes of the pure microfiber, respectively [21]. With the help of Finite Difference Time Domain simulations, we confirm that a 10-μm-long linear taper is sufficient to ensure a nearly adiabatic conversion of the signal/idler mode, with a total out-coupling loss of less than 0.3 dB. The in-coupling loss of the pump mode is found to be below 1.5 dB in few-microns-long tapers. Although a fraction of the pump is converted to unwanted modes in such a nonideal adiabatic transition, this in-coupling loss does not have any significant effect on the considered SPDC processes: the other pump modes are not phase matched with any signal or idler modes in the wavelength range of interest, and therefore they do not contribute to the SPDC process in our devices.

In the limit of an undepleted pump field, assuming low probability of photon-pair production per pump pulse ($|\nu|^2 \ll 1$), the SPDC process can be described by its output state in the following form: $|\psi\rangle \approx |\text{vac}\rangle + \nu\,|\psi_2\rangle$, where $|\text{vac}\rangle$ is the vacuum state and the two-photon state function is given by [12,26]

$$|\psi_2\rangle = \iint d\omega_s d\omega_i\, \alpha(\omega_s+\omega_i)\Phi(\omega_s,\omega_i)\,|\omega_s\rangle\,|\omega_i\rangle\,. \qquad (1)$$

In the above expression $|\omega_s\rangle$ and $|\omega_i\rangle$ are one-photon Fock states in the signal and idler modes at the respective frequencies ω_s and ω_i, and $\alpha(\omega_p = \omega_s + \omega_i)$ is the spectral amplitude of the pump pulse, for which we assume a Gaussian expression with a bandwidth of $\Delta\lambda \sim 10$ nm. The normalization of pump spectral amplitude is such that $|\alpha|^2$ gives the number of pump photons per unit pump bandwidth. The phase-matching function $\Phi(\omega_s,\omega_i)$ is defined as [27]

$$\Phi(\omega_s,\omega_i) = \int_0^L \rho_2(\omega_s,\omega_i,y)S(\omega_s,\omega_i,y)dy, \qquad (2)$$

$$S(\omega_s,\omega_i,y) = \exp\left[i\int_0^y \Delta\beta(\omega_s,\omega_i,u)du\right], \qquad (3)$$

where $\Delta\beta = \beta_p - \beta_s - \beta_i$ is the mismatch between propagation constants of the pump, signal, and idler waves; L is the overall length of the structure; and the nonlinear coefficient ρ_2 is determined by the overlap of the mode profiles and the second-order nonlinear tensor $\hat{d}^{(2)}$ [21,26]:

$$\rho_2 = \frac{\epsilon_0}{8\hbar\sqrt{N_pN_sN_i}}\iint_{WG}(\mathbf{e}_p^*\cdot\hat{d}^{(2)}\mathbf{e}_s\mathbf{e}_i)dxdz, \qquad (4)$$

$$N_j = \frac{1}{4\hbar\omega_j}\iint_{-\infty}^{\infty}(\mathbf{e}_j\cdot\mathbf{h}_j^* + \mathbf{e}_j^*\cdot\mathbf{h}_j)dxdz, \qquad (5)$$

where $j = p, s$, and i, and the integration in Eq. (4) is carried out in the LN part of the structure, while the nonlinear tensor $\hat{d}^{(2)}$ is modified inside the PE region [28], as discussed below. Electric and magnetic field profiles $\mathbf{e}_j$ and $\mathbf{h}_j$, together with the respective propagation constants β_j, are obtained with the commercial Maxwell solver package COMSOL Multiphysics.

First, we focus on structures having a fixed cross section and no PE channel. In this circumstance, the coefficients ρ_2 and $\Delta\beta$ are constant along the interaction length, resulting in the conventional sinc-shaped phase-matching function in

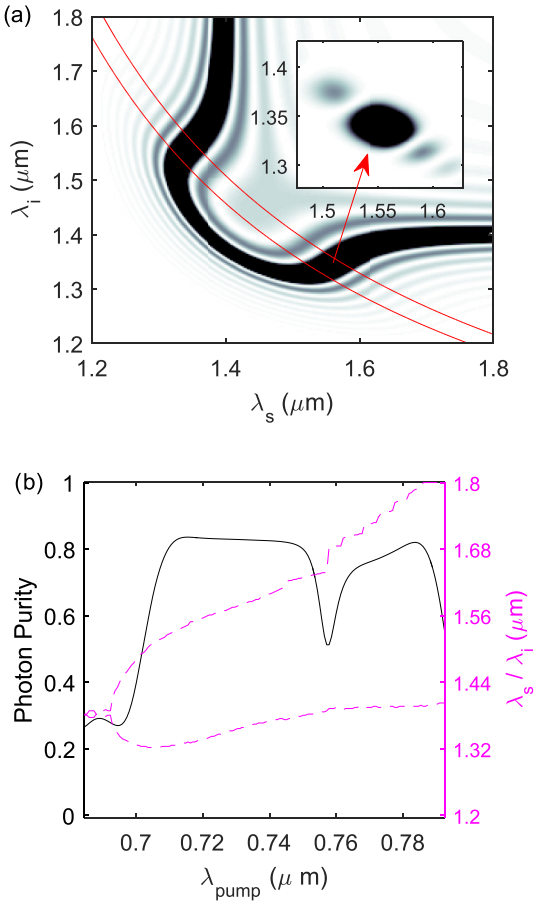

FIG. 3. Photon-pair generation in the structure with the fixed cross section of $D = 1.44$ μm, $W = 0.51$ μm, and $L = 200$ μm and without a PE channel. (a) Intensity of the phase-matching function $|\Phi|^2$, as a function of signal and idler photon wavelengths. Red contour lines indicate the pump function α for $\lambda_{\text{pump}} = 0.72$ μm and $\Delta\lambda = 12$ nm. The inset shows the corresponding JSA intensity. (b) Purity of the generated photons as a function of pump wavelength. The dashed lines indicate the corresponding signal and idler wavelengths. The sharp drop in purity at $\lambda_{\text{pump}} \approx 0.76$ μm is caused by a strong dispersion of the ρ_2 coefficient around that wavelength.

Eq. (2):

$$\Phi(\omega_s,\omega_i) = \rho_2 e^{i\Delta\beta L/2} L\,\text{sinc}\,(\Delta\beta L/2), \tag{6}$$

with the peak determined by the phase-matching condition $\Delta\beta = 0$ [see Fig. 3(a)]. In the previous work [21] we have demonstrated that the mode hybridization between microfibers and the LNOI waveguide makes it possible to achieve phase matching across a broad spectral region, adjustable by geometrical parameters of the structure. In Fig. 2 the hybridization of the two pump modes (dashed curves) is illustrated; the associated avoided crossing of the two modes enables phase matching with a signal or an idler mode (solid curve). Also, the hybridization-induced shaping of modes, shown in the inset of Fig. 2, in combination with the PE-channel-assisted modulation of the $\hat{d}^{(2)}$ tensor, enables comprehensive control of the magnitude and sign of the nonlinear coefficient ρ_2 [see Eq. (4)]. Here we benefit from the combination of the above two factors to facilitate an efficient SPDC process in a compact structure and adjust the wavelength of the generated photons to the desired specifications. In particular, in Table I we identify several possible geometries to produce high-purity photons at wavelengths around 1.55 μm from the pump in the vicinity of 0.72 μm, accessible with a tunable Ti:sapphire pulsed oscillator.

TABLE I. Examples of structure to generate high-purity photons in the vicinity of $\lambda_s = 1.55$ μm.

Geometry	Max purity		High purity range
(D, W) (μm)	$\mathcal{P}$	λ_s [λ_i] (μm)	λ (μm) for $\mathcal{P} > 0.8$
(0.7, 0.42)	0.85	1.55 [1.25]	$1.52\,[1.25] < \lambda_{s,i} < 1.6\,[1.3]$
(0.9, 0.46)	0.85	1.61 [1.28]	$1.57\,[1.26] < \lambda_{s,i} < 1.64\,[1.32]$
(1.44, 0.51)	0.84	1.54 [1.33]	$1.53\,[1.32] < \lambda_{s,i} < 1.63\,[1.38]$

The product of the pump spectral amplitude and the phase-matching function $\alpha(\omega_s + \omega_i)\Phi(\omega_s,\omega_i)$ inside the integral in Eq. (1) defines the joint spectral amplitude (JSA) of the generated photon pair. Generally it cannot be factorized, and the resulting state cannot be represented as a product state separable with signal and idler components. The degree of correlation in the output bipartite state can be analyzed by decomposing the JSA function into a weighted sum of separable functions (Schmidt decomposition): $\alpha(\omega_s + \omega_i)\Phi(\omega_s,\omega_i) = \sum_k \sqrt{b_k} u_k(\omega_s) v_k(\omega_i)$. The degree of correlation sets the photon purity, which can be calculated from the expansion coefficients: $\mathcal{P} = \sum b_k^2/(\sum b_k)^2$, $0 \leqslant \mathcal{P} \leqslant 1$, with $\mathcal{P} = 1$ corresponding to a pure heralded state [29–31]. In Fig. 3(b) the predicted purity of heralded photons is plotted as a function of pump wavelength for a particular geometry with $D = 1.44$ μm, $W = 0.51$ μm, and $L = 200$ μm. The corresponding wavelengths of signal and idler photons are indicated with the dashed curves. This compact structure allows generation of high-purity heralded single photons with $\mathcal{P} > 0.8$ in a wide spectral range: 1.53 μm $< \lambda_s < 1.63$ μm.

With several geometrical parameters available for tuning the phase-matching point, the proposed hybrid structure offers a great degree of design flexibility. Particularly, by simultaneously adjusting the fiber diameter D and the LNOI waveguide width W within a fairly large range, we are able to maintain high purity of heralded photons in the desired wavelength range. Table I lists some examples of geometries and the photon wavelengths generated with the highest purity in a 200-μm-long device.

The side lobes of the sinc-shaped phase-matching function in Eq. (6), clearly visible in Fig. 3(a), represent the major obstacle for achieving even higher purity of heralded photons. To suppress these side lobes without increasing the overall length of the device, one can adopt a variable strength of nonlinear interaction along the propagation distance. The in- and out-coupling tapers of the LNOI waveguide designed for adiabatic coupling between microfiber and hybrid structure modes, as illustrated in Fig. 1, could help to improve the photon purity, as they simultaneously provide an effective apodizing of the nonlinearity. However, the phase matching is also affected by variable LNOI waveguide width, so that both $\Delta\beta$ and ρ_2 factors in the phase-matching function Eq. (2) become intrinsically linked functions of the y coordinate. Our

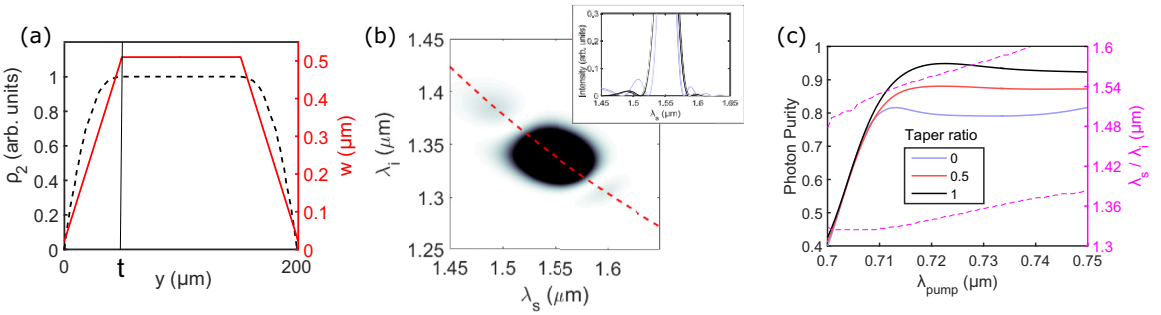

FIG. 4. Photon-pair generation in the structure with $D = 1.44\ \mu$m, $W = 0.51\ \mu$m, $L = 200\ \mu$m, and the additionally inserted tapered PE channel. (a) Width and ρ_2 profile of a generic taper. (b) Intensity of the JSA in the structure with taper ratio $2t/L = 1$ showing great suppression of secondary lobes; pump bandwidth is set to $\Delta\lambda = 14$ nm. The inset shows the cross section of the JSA intensity (bold curve) along the line of the constant pump $\lambda_{\text{pump}} = 0.72\ \mu$m, as indicated by the dashed curve in the main figure. The same cross section without the PE channel is shown in the inset by the gray curve. (c) Photon purity as a function of pump wavelength for different taper ratios.

numerical analysis indicates that, for short tapers occupying up to 20% of the total length, a few percent improvement in purity can be achieved. However, when the taper length is further increased, the negative effect due to the variation of $\Delta\beta$ starts to dominate and drags the purity down.

To optimize the hybrid structure for maximally uncorrelated photons requires independent control of the linear and nonlinear responses. This can be done by the introduction of a PE channel in the LNOI waveguide. The method of proton exchange in bulk lithium niobate is a mature technology which has been investigated for fabricating low-loss integrated photonic devices [25,32–34]. This process creates a small change to the refractive index of the crystal (<4%) [23], but has been observed to drastically reduce or completely eliminate χ_2 nonlinearity of LN [35] depending on the crystallographic phase of PE-LN. Designing a longitudinal profile $w(y)$ of the fixed-depth PE channel, we thus can manipulate the effective nonlinearity of the structure, while introducing only negligible changes to the linear dispersion factor $\Delta\beta$. In addition, this flexibility allows for the nonlinearity to be totally suppressed in the in- and out-coupling tapers, while the linear dispersion is managed for adiabatic out-coupling of the generated photons.

According to Ref. [23], for a relatively shallow depth d of the PE channel, the lateral diffusion could be ignored, so we adopted the rectangular profile of the PE region in our calculations (see inset in Fig. 1). As an example, in Fig. 4(a) the variation of the ρ_2 coefficient induced by insertion of the PE channel with a linearly tapered width between $w = 22$ and 510 nm over the taper length t in the geometry with $D = 1.44\ \mu$m and $W = 0.51\ \mu$m (cf. Fig. 3) is illustrated. By increasing the taper ratio $2t/L$ of the PE channel, a significant suppression of the side lobes of the JSA function is observed over the fixed propagation length of $L = 200\ \mu$m, as shown in Fig. 4(b). In Fig. 4(c) photon purity as a function of pump wavelength is plotted for different PE taper ratios. A significant improvement is observed for larger tapers, with the maximal photon purity reaching at least $\mathcal{P} = 0.95$ at the photon wavelength of $\lambda_s = 1.56\ \mu$m ($\lambda_i = 1.34\ \mu$m). We emphasize that this result is obtained with the simple linear tapering of the PE channel, and it can be further improved by adopting more sophisticated tapers $w(y)$ to tailor the optimal profile of the nonlinearity [19,20]. Considering the number of photon pairs created per pump pulse $N = \langle\psi_2|\psi_2\rangle$, for this structure we estimate a generation efficiency of $\eta \sim 2.5 \times 10^{-9}$ photon pairs per pump photon.

To summarize, we propose an architecture for efficient, compact, and tunable SPDC-based sources of high-purity heralded photons. The key advantages of our scheme are the following: native integration with fiber optics systems; strong second-order nonlinearity leading to high count rates of photon production; compact footprint due to direct (as opposed to quasi-) phase matching; ability to engineer dispersion and nonlinearity profiles independently via a lithographically defined PE channel; scalability and ability to adjust the spectral range of generated photons; and transverse and laminar (as opposed to longitudinal) nanostructuring offering easier and more precise fabrication. Furthermore, we believe that LNOI represents a convenient platform for further developments of quantum photonic circuits, including integration of our setup into compact spatial multiplexing schemes to enhance photon count rate.

All data created during this research are openly available from the Ref. [36].

This work was supported by the U.K. EPSRC Quantum Technology Hub "Networked Quantum Information Technologies" (Grant No. EP/M013243/1) and the National Natural Science Foundation of China (Grants No. 61575218 and No. 61275044).

[1] M. A. Nielsen and I. L. Chuang, *Quantum Computation and Quantum Information* (Cambridge University, Cambridge, England, 2010).

[2] J. L. O'Brien, Science **318**, 1567 (2007).

[3] P. Kok, W. J. Munro, K. Nemoto, T. C. Ralph, J. P. Dowling, and G. J. Milburn, Rev. Mod. Phys. **79**, 135 (2007).

[4] D. C. Burnham and D. L. Weinberg, Phys. Rev. Lett. **25**, 84 (1970).
[5] C. K. Hong, Z. Y. Ou, and L. Mandel, Phys. Rev. Lett. **59**, 2044 (1987).
[6] P. G. Kwiat, K. Mattle, H. Weinfurter, A. Zeilinger, A. V. Sergienko, and Y. Shih, Phys. Rev. Lett. **75**, 4337 (1995).
[7] S. Tanzilli, H. De Riedmatten, W. Tittel, H. Zbinden, P. Baldi, M. De Micheli, D. B. Ostrowsky, and N. Gisin, Electron. Lett. **37**, 26 (2001).
[8] A. B. U'Ren, C. Silberhorn, K. Banaszek, and I. A. Walmsley, Phys. Rev. Lett. **93**, 093601 (2004).
[9] P. J. Mosley, A. Christ, A. Eckstein, and C. Silberhorn, Phys. Rev. Lett. **103**, 233901 (2009).
[10] J. W. Silverstone, D. Bonneau, K. Ohira, N. Suzuki, H. Yoshida, N. Iizuka, M. Ezaki, C. M. Natarajan, M. G. Tanner, R. H. Hadfield, V. Zwiller, G. D. Marshall, J. G. Rarity, J. L. O'Brien, and M. G. Thompson, Nat. Photonics **8**, 104 (2014).
[11] J. He, A. S. Clark, M. J. Collins, J. Li, T. F. Krauss, B. J. Eggleton, and C. Xiong, Opt. Lett. **39**, 3575 (2014).
[12] W. P. Grice and I. A. Walmsley, Phys. Rev. A **56**, 1627 (1997).
[13] W. P. Grice, A. B. U'Ren, and I. A. Walmsley, Phys. Rev. A **64**, 063815 (2001).
[14] P. J. Mosley, J. S. Lundeen, B. J. Smith, P. Wasylczyk, A. B. U'Ren, C. Silberhorn, and I. A. Walmsley, Phys. Rev. Lett. **100**, 133601 (2008).
[15] R.-B. Jin, R. Shimizu, K. Wakui, H. Benichi, and M. Sasaki, Opt. Express **21**, 10659 (2013).
[16] A. Valencia, A. Ceré, X. Shi, G. Molina-Terriza, and J. P. Torres, Phys. Rev. Lett. **99**, 243601 (2007).
[17] O. Kuzucu, F. N. C. Wong, S. Kurimura, and S. Tovstonog, Phys. Rev. Lett. **101**, 153602 (2008).
[18] A. Eckstein, A. Christ, P. J. Mosley, and C. Silberhorn, Phys. Rev. Lett. **106**, 013603 (2011).
[19] A. M. Brańczyk, A. Fedrizzi, T. M. Stace, T. C. Ralph, and A. G. White, Opt. Express **19**, 55 (2011).
[20] A. Dosseva, L. Cincio, and A. M. Brańczyk, Phys. Rev. A **93**, 013801 (2016).
[21] A. Gorbach and W. Ding, Photonics **2**, 946 (2015).
[22] G. Poberaj, H. Hu, W. Sohler, and P. Günter, Laser Photonics Rev. **6**, 488 (2012).
[23] L. Cai, R. Kong, Y. Wang, and H. Hu, Opt. Express **23**, 29211 (2015).
[24] H. Hu, R. Ricken, and W. Sohler, Opt. Express **17**, 24261 (2009).
[25] L. Cai, Y. Wang, and H. Hu, Opt. Lett. **40**, 3013 (2015).
[26] Z. Yang, M. Liscidini, and J. E. Sipe, Phys. Rev. A **77**, 033808 (2008).
[27] L. Cui, X. Li, and N. Zhao, Phys. Rev. A **85**, 023825 (2012).
[28] Y. N. Korkishko, V. A. Fedorov, and F. Laurell, IEEE J. Sel. Top. Quantum Electron. **6**, 132 (2000).
[29] C. K. Law, I. A. Walmsley, and J. H. Eberly, Phys. Rev. Lett. **84**, 5304 (2000).
[30] K. W. Chan, C. K. Law, and J. H. Eberly, Phys. Rev. A **68**, 022110 (2003).
[31] S. L. Braunstein and P. van Loock, Rev. Mod. Phys. **77**, 513 (2005).
[32] M. L. Bortz and M. M. Fejer, Opt. Lett. **16**, 1844 (1991).
[33] K. R. Parameswaran, R. K. Route, J. R. Kurz, R. V. Roussev, M. M. Fejer, and M. Fujimura, Opt. Lett. **27**, 179 (2002).
[34] H. Lu, B. Sadani, G. Ulliac, C. Guyot, N. Courjal, M. Collet, F. I. Baida, and M.-P. Bernal, Opt. Express **21**, 16311 (2013).
[35] M. L. Bortz, L. A. Eyres, and M. M. Fejer, Appl. Phys. Lett. **62**, 2012 (1993).
[36] University of Bath data archive at http://doi.org/10.15125/BATH-00320.